



HAL
open science

Chemical stability of caesium iodide deposits in air/steam atmosphere

Dorel Obada, Houssam Hijazi, Jean-François Paul, Laurent Gasnot, Anne
Cecile Gregoire, Anne Sophie Mamede, Laurent Cantrel

► **To cite this version:**

Dorel Obada, Houssam Hijazi, Jean-François Paul, Laurent Gasnot, Anne Cecile Gregoire, et al..
Chemical stability of caesium iodide deposits in air/steam atmosphere. *Journal of Hazardous Materi-
als*, 2020, 409, pp.124519. 10.1016/j.jhazmat.2020.124519 . hal-03539663

HAL Id: hal-03539663

<https://hal.science/hal-03539663>

Submitted on 21 Jan 2022

HAL is a multi-disciplinary open access archive for the deposit and dissemination of scientific research documents, whether they are published or not. The documents may come from teaching and research institutions in France or abroad, or from public or private research centers.

L'archive ouverte pluridisciplinaire **HAL**, est destinée au dépôt et à la diffusion de documents scientifiques de niveau recherche, publiés ou non, émanant des établissements d'enseignement et de recherche français ou étrangers, des laboratoires publics ou privés.



Distributed under a Creative Commons Attribution - NonCommercial - NoDerivatives 4.0
International License

1 **Chemical stability of caesium iodide deposits in air/steam atmosphere**

2 D. Obada^{a,b}; H. Hijazi^{a,b}, J.-F. Paul^b, L. Gasnot^c, A.-C. Grégoire^a, A.-S. Mamede^b, L. Cantrel^a

3 ^a Institut de Radioprotection et de Sûreté Nucléaire, Pôle Sûreté Nucléaire, CEN Cadarache,
4 Saint Paul lez Durance F-13115, France

5 ^b Univ. Lille, CNRS, Centrale Lille, Univ. Artois, UMR 8181 - UCCS - Unité de Catalyse et Chimie
6 du Solide, F-59000 Lille, France

7 ^c Univ. Lille, CNRS, UMR 8522 - PC2A - Physicochimie des Processus de Combustion et de
8 l'Atmosphère, F-59000 Lille, France

9 **Abstract**

10 Iodine compounds that may be released in case of severe nuclear accident will have important
11 radiotoxicity if they are disseminated in air. One of the most important iodine species is CsI that is
12 deposited on the surfaces of the reactor coolant system. However, depending on the conditions, CsI
13 can volatilize or react with oxidants to produce $I_{2(g)}$. Theoretical and experimental studies
14 demonstrate that the oxidation of iodide depends on the temperature and in the presence of
15 oxidants in the gas. It is also slightly influenced by the crystallinity of the CsI particles and the nature
16 of the support. In case of a high temperature deposition, the iodine release started at temperature
17 lower than 300°C. For the CsI vapour and aerosol depositions, the iodine is detected only at
18 temperature above 450 °C and become very important above 550 °C.

19 **Key words**

20 Fission products, re-vaporization, severe nuclear accident, DFT calculations.

22 **1. Introduction**

23 In case of a severe accident (SA) occurring in a Pressurized Water Reactor (PWR), volatile radioactive
24 fission products (FPs), such as caesium and iodine, are released from the degraded fuel. They are
25 transported through the reactor coolant system (RCS) and the containment building and can be
26 released into the environment via direct leakages of the nuclear containment and/or by the
27 containment venting process in case of overpressure. As a result, these FPs can contribute to the
28 radiological consequences for the population in the short term for iodine and the long-term for
29 caesium.

30 In order to simulate an accidental scenario and predict the release of FPs, the ASTEC (Accident
31 Source Term Evaluation Code) calculation code has been developed by the French Institute for
32 Radiological Protection and Nuclear Safety (IRSN). In order to get predictive simulations[1], a
33 comprehensive knowledge of all the phenomena occurring in a PWR during a severe accident
34 situation is necessary. Considerable advances have been made in the field of understanding the
35 behaviour of volatile FPs such as iodine after their release from the damaged core, thanks to
36 experimental programs such as Phébus-FP [2] and other experimental works devoted to FP
37 behaviour[3] and subsequent modelling works.

38 Nevertheless, some phenomena are not accounted for yet by the simulation tools and it is difficult to
39 predict their outcome, mostly because of a lack of experimental and/or theoretical data. It is the case
40 with the re-vaporization of FPs deposits from the surface of the RCS. FPs will form deposits on the
41 surface of the RCS by different mechanisms, the most important of which are vapour condensation
42 and thermophoresis as predicted by Hidaka *et al.* [4] and Maruyama *et al.* [5], as well as gravity
43 deposition. The Phébus-FP experimental program has shown that Cs and I can significantly deposits
44 in the RCS [6]. The main identified iodine compounds is CsI – resulting from condensation of CsI
45 vapours in the 600-650°C temperature range (as expected from thermodynamic calculations and
46 simulation with severe accident software as the ASTEC code [1]). Other condensed iodine form were
47 identified too, but their nature could not be fully unravell ed – they are expected to be metallic iodide
48 of control rod material (Cd or Ag). Moreover, it was determined from Phébus tests, that Cs
49 remobilization can reach up to 75% of the initial deposit in certain conditions [2]. More recently, in
50 the aftermath of the Fukushima Daiichi accident, delayed releases for iodine and caesium have been
51 detected several days after the accident [7] [8], and are believed to be related to the chemical re-
52 vaporization of caesium and iodine containing deposits.

53 In the past several attempts have been made to understand the phenomenon of FPs remobilization.
54 As a follow-up of the Phebus-FP tests, a series of research programs have been launched by several
55 institutions. The studies focused mainly on the re-vaporization of caesium in a wide range of
56 temperature and carrier gas conditions; iodine behaviour, for its part, was less studied. The studied
57 precursor was mostly CsOH [8-12], less frequently CsI [10, 13, 14-16].

58 As for caesium, AEA-T [9] studied the re-vaporization of synthetic CsOH deposits in a flow reactor at
59 temperatures reaching up to 1100°C, analysing the mass balance and surface interaction between
60 caesium and the substrate made of 304 SS steel. Auvinen *et al.* [10] have studied the vaporization of
61 CsOH and CsI powders from stainless steel crucibles. The samples were traced with radioactive Cs
62 (¹³⁴Cs or ¹³⁷Cs), which allowed establishing a release kinetics thanks to γ -spectrometry
63 measurements. The two studies used steam as carrier gas and it was established that the Cs re-
64 vaporization starts at \approx 500°C. Bottomley *et al.* [11] and Knebel *et al.* [12] performed online γ -
65 spectrometry measurements of ¹³⁷Cs from deposits issued from the Phebus-FP tests (vapour
66 deposition at temperatures up to 700°C), which are as realistic as possible. However the initial
67 composition of the deposits, as well as the surface state of the stainless steel substrate is not well
68 defined. The results show that in steam Cs is released starting from 550°C, whereas in air atmosphere
69 the release occurs at a lower temperature, as low as 300°C.

70 The studies dealing with CsI were aimed at investigating conditions leading to CsI decomposition and
71 subsequent gaseous iodine releases. Experiments performed by Kalilainen *et al.* [13] allowed a better
72 understanding of the re-vaporized Cs and I distribution between gaseous and aerosol forms, thanks
73 to the use of liquid scrubbers and filters adapted for each type of material. It was found that up to
74 27% of initial iodine content is released in gaseous form in an argon/steam atmosphere, and that it
75 decreases with the introduction of hydrogen in the carrier gas. Shibazaki *et al.* [14] performed tests
76 with CsI in steam and concluded that it starts re-vaporizing at \approx 490°C and is released mainly as CsI.
77 Berdonosov *et al.* [15] [16] conducted small-scale tests to further study the chemical nature of the
78 released gaseous iodine. By heating CsI in air up to 1250°C, the formation of gaseous molecular
79 iodine I₂ has been observed, the higher the temperature the larger the amount. Kulyukhin *et al.* [17]
80 studied the hydrolysis of CsI in presence of molecular oxygen in the 630-1300°C range and the

81 formation of I_2 has been also confirmed, indirectly. However, some key parameters were not fully
82 investigated in those studies. For instance, the FP deposit-substrate interaction was not always taken
83 into account. Indeed, if some studies featured stainless steel substrates [10, 13] the initial surface
84 state is not documented. Some studies featured even substrates not representative of the RCS (glass
85 or platinum [14-16], alumina [10]). Secondly, the process of CsI deposition was not always examined
86 as most of studies were performed with commercial CsI powder; CsI vapour and aerosol deposition
87 were only considered in [13]. Finally, the influence of carrier gas composition and thermal conditions
88 on re-vaporization were not fully investigated: most of studies considered steam or steam/hydrogen
89 atmospheres which are more representative of early degradation phase during SA, whereas air was
90 only considered in [14-16], but in the latter case, the thermal treatment (flash heating up to 1250°C)
91 seems unrealistic regarding late phase SA conditions.

92 From the theoretical point of view, to the best of our knowledge, the revaporisation and the
93 chemical reactivity of CsI aerosols had only been studied by H. Hijazi ([18]). The other theoretical
94 studies in a nuclear frame focused on the gas reactivity of iodine species or on chemical
95 stability/reactivity of caesium species ([19] [20] [21] [22] [23] [24] [25] [26] [27]). Severe accident
96 simulations in the RCS are based on chemical equilibrium in gas phase thus ab initio computations
97 were performed on the speciation at the equilibrium of the compound containing iodide or caesium.
98 The gas inorganic chemistry involves mainly molecular iodine (I_2), monoatomic iodine radicals (I^*) and
99 iodine oxides (IO_x). The conversion between the species are fast and are favoured by oxidants such as
100 nitrogen oxide and by visible light or radiation. The interaction with water occurs through the
101 formation of hydrogen bonds and hydrogen transfer between acidic and radical species. The
102 reactivity of caesium species in the gas phase has not been studied extensively. The reaction
103 between CsO and H_2 have been investigated by Louis at al. [28]. Based on all these studies, it is
104 possible to estimate the concentrations of some iodine and caesium species in the gas phase
105 depending on the experimental conditions [29].

106 In conclusion, data on caesium and more particularly on gaseous iodine re-vaporization are too
107 scarce and remain to be confirmed in more representative conditions to build an appropriate
108 modelling.

109 The work presented here was aimed at fill in the gap in knowledge on CsI re-vaporization in
110 conditions as representative as possible of a late phase of a SA scenario, in terms of: i/ substrate
111 nature (pre-oxidized 304L and 316 L stainless steel which correspond to RCS steel composition) ii/
112 deposit generation (reproducing the different temperature deposition processes as in [13]: high
113 temperature deposition, vapour condensation and finally aerosol impaction with realistic deposited
114 amounts ~i.e. few mg/cm^2) iii/ re-vaporization thermal conditions (with heating up to 750 °C), iv/
115 presence of air (steam/air mixtures), since air is susceptible to penetrate in the RCS in case of an air-
116 ingress accidental scenario[30]. We aimed at a better assessment of gaseous iodine release with the
117 identification of re-vaporized species and their kinetics.

118 Preliminary results of the study have been published before [31], [32] and were focused mainly on
119 the re-vaporization of CsI aerosol deposits in pure atmosphere (air or steam). This paper expands on
120 the previous results and presents the re-vaporization of different types of CsI deposits in a mixed
121 air/steam carrier gas as well as investigates the release kinetics for gaseous molecular iodine. Special
122 attention was brought to the substrate nature, and its preparation in order to obtain a surface state

123 as similar as possible of RCS inner parts after several hours of oxidation in steam conditions [32] [33]
124 at high temperature. The surfaces before and after deposit re-vaporization process were carefully
125 determined by combining X-Ray Photoelectron Spectroscopy (XPS) and Time-of-Flight Secondary Ion
126 Mass Spectrometry (ToF-SIMS). The release rate was monitored by thermogravimetric analysis (TGA)
127 and the nature of released vapours was determined. Also, the release kinetics for molecular iodine
128 has been studied by a novel spectroscopic technique, Incoherent Broadband Cavity Enhanced
129 Absorption Spectroscopy (IBB-CEAS)[34].

130 Hereafter the article is composed of an experimental section which describes the equipment used
131 and the analytical techniques employed. The following section presents the experimental results
132 concerning the re-vaporization CsI deposits. Finally, a theoretical modelling of the experiments is
133 done, in order to improve the understanding of the reaction mechanisms.

134 2. Materials and methods

135 The experimental study is based on a multistep approach including:

- 136 - Substrate pre-oxidation;
- 137 - CsI deposits generation;
- 138 - CsI deposits thermal treatment.

139 After each step the samples are characterized in order to establish the surface state of the substrate
140 (XPS, ToF-SIMS), deposit quantity (ICP-MS), mass balance for caesium and iodine after re-
141 vaporization (ICP-MS, TGA, UV-Visible spectroscopy).

142 2.1. Substrate pre-oxidation

143 304L stainless steel coupons (8×15×2 mm), whose composition is presented in Table 1, underwent a
144 thermal treatment in a controlled atmosphere in a flow reactor to reproduce as close as possible the
145 surface state of the RCS inner part in SA conditions. The thermal treatment consisted in exposing the
146 coupons to a flow of argon/steam (% vol. 50/50) at 750 °C during 24 h. The heating rate was 5°C/min
147 and steam was injected at 150 °C. The total gas flow rate was fixed at 1 L_n/min¹ at standard
148 conditions. 316L foils (100×500×0.075 mm, see composition in Table 1) were pre-oxidized in the
149 same thermal conditions and process gas composition, except that the total gas flow was 4 L_n/min at
150 standard conditions. In both case, the carrier gas flow was laminar and steam proportion in the flow
151 (50%) is large enough to allow equivalent oxidation conditions of the stainless steel surfaces.

152 **Table 1. General composition (wt. %) of the 304L and 316L stainless steels ([32])**

	C	Cr	Fe	Mn	Mo	Ni	Si	Other
304L	0.03	18.0-20.0	base	2.0		8.0-12.0	1.0	P,S<0.045
316L	0.03	16.0-18.0	base	2.0	2.0-3.0	10.0-14.0	0.75	P,S<0.025

153

154 2.2. CsI deposits generation

¹ The gas flow rates are given for the reference conditions: 273 K, 101325 Pa and are thus noted L_n/min

155 In this study three types of CsI deposits were considered: aerosols impactation at room temperature by
156 Room temperature (RT) aerosol impactation, high-temperature vapour deposition/condensation and
157 temperature aerosol deposition.

158 The CsI impacted aerosols were obtained following the procedure described by Obada *et al.* [33]
159 which consists in nebulizing a concentrated CsI aqueous solution. The obtained wet aerosols are then
160 dried in a strong argon flow (10 L/min) and afterwards impacted on the pre-oxidized 304L coupons
161 placed in an exposition chamber (8 coupons per batch).

162 The high-temperature CsI deposits were generated using a high-temperature furnace. The thermal
163 profile of the heated alumina tube is bell-shaped, with a 5 cm isotherm zone at the centre. An
164 alumina crucible (5 cm) containing CsI powder (Acros Organics, 99.9%) was placed inside a 1 m long
165 alumina tube (30 mm inner diameter), inserted in the furnace. The crucible was placed in the
166 isothermal zone. Downstream the alumina tube wall was lined by a 316L pre-oxidized foil. The
167 crucible was heated up to 750°C (5°C/min rate) and the temperature was maintained at 750°C for 6
168 hours. The carrier gas was a mixture of argon and steam (% vol. 20/80) at total gas flow of 0.62
169 L_n/min. The 316L foil was placed in a strong thermal gradient as such vaporized CsI was transported
170 by the carrier gas and was deposited along the pre-oxidized 316L foil in a wide temperature range
171 (from 750 to 150°C)_ covering thus all deposition processes from a high temperature vapour
172 deposition (above 620°C), vapour condensation (between 620 and 400°C) and aerosol deposition
173 (below 440°C). Downstream of the alumina tube was a series of two liquid scrubbers containing an
174 alkaline solution (NaOH 0.1M) dedicated for steam condensation and trapping any non-deposited
175 material. The line was terminated by an integral filter. After the test, the 316L foil is recovered and
176 divided into several sections (~2-3 cm long and 1-2 cm large) based on a visual inspection of the
177 deposit.

178 The deposited mass is determined after leaching one of the 304L coupons (wet deposition) and a
179 selection of small 316L samples, cut from the foil (high temperature deposit generation) in selected
180 area, in alkaline media (NaOH 0.1 M) for I and Cs recovery in solution followed by elemental I and Cs
181 determination by Inductively Coupled Plasma – Mass Spectrometry (ICP MS –Varian 810 MS).

182 **CsI deposits thermal treatment**

183 The re-vaporization of CsI deposits from pre-oxidized stainless steel surfaces were carried out in a
184 thermogravimetric analysis (TGA) device as described by Obada *et al.* [31]. Given the TGA furnace
185 geometrical constraints (inner diameter of less than 1 cm), only the 304L coupons could be thermally
186 treated in this device. The thermal treatment consisted in heating the samples up to 750°C (except
187 for some tests, where samples were heated up to 970°C or 550°C only) at a rate of 5°C/min and hold
188 for 1 hour, before cooling down by natural convection. The rate of the heating ramp is a compromise
189 between chemical equilibrium conditions and test duration (2-3 hours) [35]. During the thermal
190 cycle, the sample is swept by a low carrier gas flow either composed of synthetic air (30 mL_n/min) or
191 air/argon/steam mixtures (air/steam mixture featuring a total flow rate of 30 mL_n/min; argon flow
192 rate set at 70 mL_n/min). Air/steam mixtures were injected at temperature above 150°C and switched
193 off during the cooling phase (below 400°C).

194 The main outcome of the TGA tests is the onset temperature of the mass loss linked to the start of
195 the re-vaporization process. The overall mass change (loss) cannot be considered as a measure of CsI

196 re-vaporization as the oxidation of the substrate during the thermal treatment may counterbalance
197 the mass loss linked to re-vaporization. On the more, the inner alumina liner of the TGA device
198 presents an important reduction in diameter (from 1 cm to 0.4 cm (Obada [2017])) just downstream
199 of the sample, probably inducing at its vicinity some perturbation in the fluid flow which may
200 enhance deposit retention on the sample.

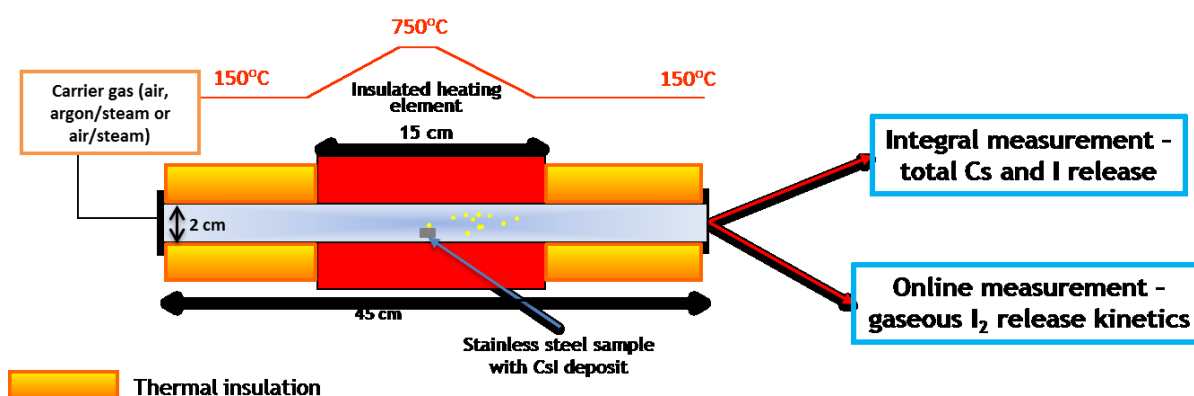
201 To complement the results obtained by TGA, the RIGolo (**Re**-vaporization of **I**odine in **G**aseous form
202 and “piccolo”=“small” in Italian) experimental device has been developed with a double purpose:

- 203 - Establish the nature and quantity of released iodine-containing species;
- 204 - Determine the release kinetics for gaseous molecular iodine.

205 It is an open flow reactor (Figure 1) composed of a tubular furnace (WATLOW ceramic heater CF-
206 964255, 15 cm) in which an alumina tube (45 cm long, 20 mm inner diameter) is inserted. The sample
207 is placed at the centre of the furnace and the carrier gas is fed up at the inlet of the test line. The
208 vaporized vapour and/or generated aerosols from the heated sample are transported by the carrier
209 gas to the line outlet. Based on the type of information searched in the experiment, the downstream
210 part of the RIGolo device has two configurations: “integral measurement” for determining the nature
211 and quantity of released iodine-containing species and “online measurement” for establishing the
212 gaseous I₂ release kinetics.

213 The “integral measurement” configuration is described by Obada *et al.* [31] and consists in
214 connecting the alumina tube outlet to a series of selective liquid scrubbers, containing a mix of
215 toluene/acidic water. It has been shown that in these conditions molecular iodine will be selectively
216 trapped in the organic phase, while inorganic iodine compounds (CsI, HI) will be trapped in the
217 aqueous phase [36] [37]. Since the detection limit of I₂ in toluene by UV-Visible spectroscopy is
218 between 2×10^{-8} and 6×10^{-7} mol/L (for the absorption wavelengths of 309 nm and 496 nm
219 respectively), it is necessary to accumulate I₂ over a long period of time (2 h), hence the experiment
220 was called “integral”.

221 The “online measurement” configuration consists in connecting the alumina tube outlet to an
222 Incoherent Broadband Cavity Enhanced Absorption Spectroscopy (IBB-CEAS) device dedicated to
223 monitor online the gaseous molecular iodine concentration, transported up to the optical cell, by
224 absorption spectroscopy in the 510-570 nm range [38] [34]. In this case the re-vaporization products
225 (gaseous species, aerosols) are diluted in an argon flow before being injected in the optical cell. The
226 technique has a low detection limit (1 ppb volumic in the gas phase) and a good temporal resolution
227 (10 s), which makes possible a kinetic study in our experimental conditions (1-2 mg of iodine re-
228 vaporized for ≈ 1 h in a 200 mL_n/min gas flow).



229

230

Figure 1. General design of the RIGolo experimental device

231 The thermal treatment in the RIGolo device is similar to the one applied in the TGA device: heating
 232 up to 750°C (rate 5°C/min) and hold for 1 hour, before cooling by natural convection. The carrier gas
 233 during the tests was either air (53 mL_n/min) or a mixture of air/steam (200 mL_n/min) of variable
 234 composition. The gas flow rates have been adjusted to the new alumina tube inner diameter, in
 235 order to have the same gas velocity above the sample as in the TGA tests.

236 2.3. Post-test analysis

237 2.3.1. Elemental mass balance determination

238 After each test, the entire facility, including the stainless steel and gold coupons, was leached in
 239 alkaline media for iodine and caesium deposits recovery and elemental determination. As in [31], the
 240 solutions were analysed by ICP-MS for elemental quantification with an uncertainty of +/- 8% (at 95
 241 % confidence level). The organic phase of the liquid scrubbers has been also recovered and analysed
 242 by UV-Visible spectroscopy for quantification of I₂ in toluene, which was performed with an Agilent
 243 Cary 8454 spectrometer at 309 nm and 496 nm with an uncertainty of +/- 6% (at 95 % confidence
 244 level).

245 2.3.2. Surface Characterization Techniques

246 The sample surface was characterized by combination of X-ray Photoelectron Spectroscopy (XPS) and
 247 Time-of-Flight Secondary Ion Mass Spectrometry (ToF-SIMS). XPS provides chemical composition of
 248 less than 10 nm depth scale of the surface while the ToF-SIMS was used in depth profiling mode to
 249 reach composition up to several micrometres in depth. The morphology of the surface before and
 250 after re-vaporization was investigated by Scanning Electron Microscopy (SEM).

251 XPS measurements were carried out on a Kratos AXIS Ultra^{DLD} spectrometer equipped with a
 252 monochromatic Al K α source (1486.6 eV). Calibration was done by using the C 1s component of
 253 adventitious at BE (binding energy) = 285.0 eV. Binding energy value uncertainty is +/- 0.1 eV and
 254 uncertainty on quantitative elemental analysis is +/- 10%.

255 ToF-SIMS analyses were carried out using a ToF-SIMS 5 instrument (ION-TOF GmbH). Pulsed Bi⁺
 256 primary ions have been used for analysis (25 keV, \approx 1 pA) and O₂⁺ for sputtering (2 keV, \approx 500 nA).
 257 Given the sputter parameters, estimated sputter speed is 1.6 nm/s. Mass spectra were recorded in
 258 positive (for each sample) and negative for one sample polarity from an analysis area of 100 μ m x

259 100 μm centred into a 300 μm x 300 μm sputtered area. Charging effects, due to analysis and erosion
260 ion beam, were compensated using low energy electrons (20 eV).

261 Scanning Electron Microscopy (SEM) images were obtained using a LEO-435 VP microscope. A 20 kV
262 accelerating voltage was used giving an interaction depth above 2.5 μm^3 .

263 **2.3.3. IBB-CEAS signal interpretation and presentation**

264 The IBB-CEAS configuration and characteristics are extensively discussed in [38] and [34]. It is based
265 on the I₂ fine resolved spectrum in the 510-570 nm spectral range owing to the numerous rovibronic
266 transitions in the I₂ B \leftarrow X electronic absorption spectrum [38]. The light source is a LED emitting in the
267 480-580 nm and the detector is a CCD camera (Andor iDus).

268 As explained by Bahrini *et al.* [38] and Johansson *et al.* [34], the I₂ spectra registered by the CCD
269 detector require mathematical processing in order to separate the spectral contribution of gaseous
270 molecular iodine from the continuous component of the spectra. Moreover, for practical reasons
271 [38], a calibrated source of I₂ is analysed by the IBB-CEAS at the beginning of each experiment. Iodine
272 concentration in the sample is then displayed as the adimensional N_{rel} value which is the ratio of I₂
273 sample concentration to the calibration source concentration. Absolute concentration in the samples
274 requires to be adjusted for the sampling, calibration and dilution flow rates. In our case, as the main
275 objective is to determine the release kinetic, it was decided to stay with relative concentration. For
276 comparison purpose, the kinetic curves were rescaled based on the overall fractional release of
277 molecular iodine, whenever possible (data from integral RIGolo experiments). Hereafter the figures
278 displaying I₂ release kinetics present the rescaled N_{rel} evolution as a function of time and
279 temperature.

280 **2.3.4. DFT Calculations**

281 All DFT (density functional theory) calculations were carried out with VASP (Vienna Ab initio
282 Simulation Package [39] [40] [41]). Plane waves are used to describe the wave functions and the PAW
283 (Projector Augmented Wave) [42] method for electron-ion interactions. The energy is calculated
284 using GGA as parametrized by Perdew *et al.*, [43] and with a Methfessel-Paxton[44] smearing
285 parameter sigma set to 0.1 eV. The Kohn-Sham equations are solved self-consistently until the
286 energy difference between two successive steps is lower than 10⁻⁵ eV. The atomic positions were
287 optimized without symmetry constraints until the forces being less than 0.03 eV/Å. The electron
288 configurations [Xe] 6s1, [Kr] 4d10 5s2 5p5, [He] 2s2 2p4 and 1s1 were used for caesium, iodine,
289 oxygen and hydrogen respectively. The cut of energy was set to 450 eV and 3x3x1 or larger K-point
290 meshes [45] have been used for all the surface calculations (distance between K point smaller than
291 0.035Å⁻¹). Van der Waals interactions are included in the calculation through the TSHI formalism[46]
292 that take into account the charges on the atoms.

293 The adsorption energy (E_{ads}) is defined as the opposite of the adsorption reaction energy. A positive
294 adsorption energy is associated to an exothermic adsorption.

$$295 \quad A_{(g)} + \text{Surface} = A\text{-Surface} \quad E_{\text{ads}} = E(A_{(g)}) + E(\text{Surface}) - E(A\text{-Surface}).$$

296 **3. Experimental matrix**

297 The first tests concerning the re-vaporization of CsI aerosols (Room temperature aerosol impaction)
298 from pre-oxidized 304L or 316L substrate in presence of argon/steam have shown an integral release
299 of Cs and I [31]. As such these test conditions will serve as reference. The goal of this research was to
300 assess gaseous iodine release during re-vaporization of CsI deposits, through small-scale analytical
301 tests.

302 Stainless steels of different grades (304L or 316L) were used to represent the inner surface of the
303 RCS in general. The coupons were pretreated (pre-oxidation at 750°C in steam conditions) so as to
304 feature a surface state representative of the RCS in case of a SA. As reported in [32], the structure of
305 surface oxide is similar for both stainless steels grades and has no influence on the CsI re-
306 vaporization behaviour. In the case of 316L foils, oxide structure is slightly different, presenting an
307 outer Fe-rich layer (as opposed to a Mn-rich layer) and an inner Cr-rich layer. Nevertheless, taking
308 into account the thickness of the deposit (estimated to be in the range of 2-7 µm for 1-3 mg/cm² for
309 deposited CsI), we expected a low contribution of deposit/surface interaction on re-vaporized
310 species. Indeed, for such thick deposits, the fraction of CsI in contact with the substrate surface is
311 low.

312 Except for one test, the same thermal cycle was applied: heating at 5°C/min up to 750°C. This final
313 temperature is high enough to be able to catch every release events concerning CsI re-vaporization
314 and remains within the expected temperature range which could prevail in the RCS during a late SA
315 phase.

316 The study was focused on the two main following parameters (see table 2):

- 317 • The CsI deposition process, to be able to reproduce the different deposition zones in the RCS:
318 RT temperature aerosol impaction (simulating CsI deposition in the cold leg of the RCS), high
319 temperature vapour deposition (above 620°C, simulating a deposition in the hot leg of the
320 RCS and SG inlet), vapour condensation (620-400°C, simulating SG deposition) and
321 temperature aerosol deposition (around 400°C, SG deposition).
- 322 • The atmosphere composition featuring either air, air/steam mixtures and argon/steam. Air
323 and steam atmospheres are not representative of SA scenario but may help in understanding
324 the CsI re-vaporization behaviour and gaseous iodine production. Realistic atmospheres are
325 mixture of air/steam with a low air content. Re-vaporization of CsI aerosols (RT aerosol
326 impaction) on 304L coupons featured the largest atmosphere compositions (5 different
327 compositions as reported in table 2, from pure air contents to argon/steam). Tests were
328 performed in both TGA and RIGolo devices. Based on the results of this test series, the
329 number of tested atmospheres has been reduced for the CsI vapour deposition and vapour
330 condensation: one test in steam, one in air and one in a 20/80 air/steam atmosphere. Finally,
331 for the deposit obtained by temperature aerosol deposition (400 °C), only the pure air and
332 steam atmospheres have been retained for the re-vaporization tests, to check for
333 consistency with CsI aerosol impaction at room temperature. The tests have been performed
334 in the RIGolo device only, as the 316L foil samples were not suited for the TGA device (see
335 table2).

336 Two complementary tests were performed:

337 On test with an inert substrate to assess the contribution of deposit/surface interaction in terms of
 338 nature of re-vaporized species (especially for iodine). CsI aerosols were deposited on gold coupons by
 339 the room temperature aerosol impaction process. Tests conditions featured air atmosphere and a
 340 thermal cycle (5°C/min up to 750°C) similar to conditions 1. Tests were performed in both devices
 341 (TGA and RIGolo) to allow a complete comparison with condition 1, table 2.

342 One test with a lower final test temperature (550°C), dedicated to the observation of iodine re-
 343 vaporization kinetics at low temperature. This test was conducted with initial CsI RT aerosol deposits
 344 on a stainless steel coupon and a mixed steam/air atmosphere was applied (instead of pure air) to be
 345 more representative of a reactor case. This test was performed in the RIGolo device in the I₂ on-line
 346 monitoring configuration. The sample was initially heated up to 420°C in argon (rate 5°C/min), then
 347 the carrier gas was switched for a mixture of air/steam (% vol. 50/50). After that the sample was
 348 heated up to 550°C (rate 5°C/min) and held for 4 h before cooling by natural convection. The upper
 349 limit for temperature was chosen based on the results of Bottomley *et al.* [11], where it has been
 350 observed that Cs re-vaporization is much slower and less significant after 750-800°C.

351 **Table 2. CsI re-vaporization - Experimental matrix for test performed with thermal cycle up to 750°C at 5°C/min.**

Substrate	Deposition process	Re-vaporization carrier gas (% vol)	Experiment type (repeat)			Condition n°
			Integral ¹	Kinetic ²	TGA ³	
Pre-oxidized 304L	Aerosols impaction at room temperature	Air (100%)	x [31] (3)	x	x [31]	1
		Air/steam (50/50)	x	x		2
		Air/steam (20/80)	X (2)	x	x	3
		Air/steam (3/97)	x	x	x	4
		Argon/steam (50/50)	x[29]		x [29]	5
Pre-oxidized 316L	High-temperature vapour deposition (720-620°C)	Air (100%)	x	x		6
		Air/steam (20/80)	x			7
		Argon/steam (50/50)	x			8
	Vapour condensation (620-440°C)	Air (100%)	X (2)	x		9
		Air/steam (20/80)	X	x		10
		Argon/steam (50/50)	X			11
	Aerosols deposits (< 400°C)	Air (100%)	X			12
Argon/steam (50/50)		x			13	
Gold (Au)	RT aerosol impaction	Air (100%)	x	x	x	14

352 ¹ RIGolo with biphasic liquid scrubbers

353 ² RIGolo coupled to the IBB-CEAS

354 ³ Thermogravimetric analysis

355 4. Results

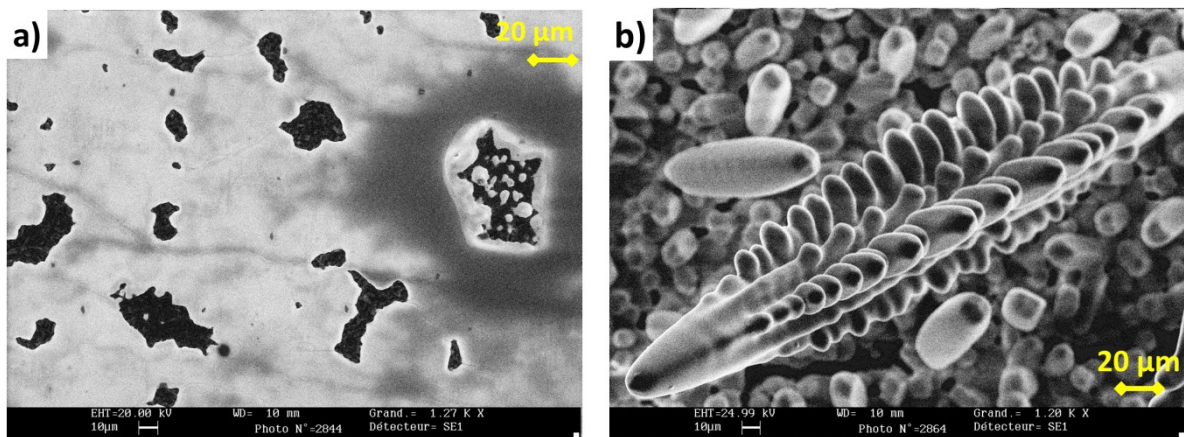
356 4.1. Deposit characterization

357 After the pre-oxidation of 304L and 316L stainless steel coupons and foil, CsI is deposited as
 358 described in section 2.2. Afterwards the size and the morphology of the deposits are characterized by
 359 SEM and the amount of deposited CsI is determined by ICP-MS after lixiviation.

360 The CsI aerosols deposits obtained by impaction at room temperature have been described by Obada
 361 *et al.* [33]. SEM analysis has revealed the presence of particles with irregular shapes and particle
 362 agglomerates with sizes from 5 to 20 µm. After several weeks, the particles also appear to hydrate,
 363 given the hygroscopic nature of CsI [47]. ICP-MS analysis has revealed similar CsI quantity among all

364 the 304L coupons of the same batch, with values ranging from 0.8 to 4.2 mg/cm² of CsI from one
365 experiment to another.

366 The Cs and I deposits obtained at high temperature, on the other hand, exhibit different sizes and
367 morphologies based on the deposition temperature. For instance, in the 720-620°C temperature
368 range, SEM analysis has revealed an amorphous deposit, homogeneously spread across the entire
369 surface of the 316L foil (Figure 2a) – corresponding to the deposition of liquid droplets. The average
370 amount of caesium and iodine per surface unit in this temperature range is about 2.9 mg/cm², as
371 determined by ICP-MS analysis. Also, the Cs/I mass ratio of 0.94 is consistent with to the theoretical
372 value (1.05) taking into account uncertainties measurement, which strongly suggests that caesium
373 and iodine were deposited as CsI. In the 620-440°C temperature range, the deposit is composed of
374 polyhedrons that range between 10 and 30 μm in size, as well as acicular particles with lateral
375 dendrites that reach several hundred microns in size (Figure 2b). The deposit in this temperature
376 range is the most important in terms of quantity, up to 8.3 mg/cm², and the Cs/I mass ratio (0.96)
377 suggests that the chemical species is CsI. Below 440°C, the deposit consists of spherical particles that
378 reach up to 4 μm in diameter (not presented here). The amount of deposit decreases progressively
379 from 4.3 mg/cm² at 440°C to 0.7 mg/cm² at 150°C. Given the Cs/I mass ratio (0.89-0.99), it is highly
380 likely that the deposit is composed of CsI.



381

382 **Figure 2. SEM images of high-temperature CsI deposit on pre-oxidized 316L foil: a) between 720-620°C and b) between**
383 **620-440°C.**

384 **4.2. Re-vaporization: identification of released and residual species and release kinetics**

385 In this chapter are presented the results of RIGolo and TGA tests in different conditions (Table 2) as
386 well as the results of the kinetics tests. Since the goal is to investigate the separate effect of different
387 parameters, the results are presented following the listed parameters: carrier gas composition,
388 deposition process, substrate nature (stainless steel vs gold) and finally low temperature re-
389 vaporization. Here the main trends will be discussed depending on the test parameters. Variability in
390 test results may occur for equivalent test conditions (and for repeats) due to inhomogenities of CsI
391 deposits.

392 **4.2.1. Influence of carrier gas composition: air vs. mixed air/steam (conditions 1 to 5)**

393 As previously reported [31] [33], the carrier gas composition during the re-vaporization phase is one
394 of the key parameters regarding the nature of re-vaporized and residual species. As such, in an

395 argon/steam carrier gas, caesium and iodine are released integrally from the surface of stainless steel
396 coupons (condition 5). The absence of gaseous iodine species at the line outlet and Cs/I ratios
397 measured downstream of the steel coupon close to ~ 1.1 (main line data), suggest a re-vaporization
398 as CsI only [31].

399 With the addition of air in the carrier gas (in increasing amounts following conditions 4, 3, 2 up to
400 pure air, condition 1), we can observe that the overall fraction of released molecular iodine (RIGolo
401 test in integral configuration) is roughly the same (~ 23 - 33% of total iodine) as soon as air is present
402 in the gas phase, except for pure air conditions featuring much higher gaseous iodine releases (up
403 75% of total iodine amount). Indeed, oxygen is always present in sufficient amount to react with
404 iodine taking into account the oxygen flow (from ~ 0.02 up to 0.7 mg/s), the test duration (2 hours of
405 heating and one hour at 750°C) and the initial iodine mass (1-2 mg) – so that the role of oxygen is
406 expected to be the same in all the cases as soon as it is present (see section 5 for theoretical part). In
407 pure air, TGA tests have shown that the release starts at 420°C on average, releases seems to be
408 delayed as soon as steam is present with onset temperatures in the 450 - 470°C range. These
409 observations (lower gaseous iodine releases and higher re-vaporization onset temperature) in
410 air/steam conditions compared to pure air condition may be owed to possible limiting effects of
411 steam which are not yet understood.

412 Concerning the residue (RIGolo tests in integral configuration), the ICP-MS analysis of the leaching
413 solutions of the stainless steel coupons has consistently revealed the absence of iodine, which
414 implies its total re-vaporization, and the presence of a residual amount of caesium. In pure air (Table
415 3, condition n°1), Cs retention amounts up to 10% of the total measured amount at the end of the
416 test. The ICP-MS analysis of the alumina tube leachate shows a Cs/I mass ratio in between ≈ 5 - 11 .
417 This feature indicates that beside CsI, Cs is mainly deposited in other chemical forms – expected to
418 be CsO as this species is the most stable from a thermodynamic point of view in the absence of
419 steam. In air/steam, Cs retention on the coupon represents up to 9% of total Cs collected mass (Table
420 3, conditions n°2 & 3). The integral experiment in conditions n°4, which featured the smallest ratio of
421 air to steam (% vol. 3/97), has resulted in a residual amount of Cs of only 1.5% . The Cs/I mass ratio in
422 the alumina tube does not vary a lot when considering all the mixed air steam conditions (1.4-1.6).
423 This value is still above the Cs/I mass ratio of CsI (1.05) and support the hypothesis that beside CsI,
424 other Cs compounds may have deposited in the main line (though in a lesser extent compared to
425 pure air condition). In presence of steam, the other expected Cs compound is CsOH.

426 A detailed surface characterization by XPS and ToF-SIMS of 304L samples after re-vaporization in air
427 or argon/steam has been discussed by Obada *et al.* [33]. The same process has been applied to the
428 304L samples obtained after re-vaporization in air/steam atmosphere and the results show evidence
429 of the formation of mixed Cs-Cr oxides, specifically Cs_2CrO_4 and $\text{Cs}_2\text{Cr}_2\text{O}_7$. This observation is
430 supported by XPS analysis which revealed the presence of two chemical forms of chromium: Cr(III)
431 and Cr(VI) oxides. Also, ToF-SIMS analysis has revealed the presence of secondary ion clusters
432 $\text{Cs}_2\text{CrO}_3^+$ and $\text{Cs}_2\text{Cr}_2\text{O}_9\text{H}^+$, which is a strong indication that the said oxides have been formed during
433 the re-vaporization process. These results demonstrate that the nature of the support affect the
434 behaviour of residual Cs+ but not that the same support participate to the iodine oxidation but that
435 in oxidizing condition, the chromium of the support can react with the air[48].

436 This test series (conditions 1 to 5) was complemented by RIGolo tests performed with the on-line
437 configuration in order to monitor I_{2g} release during the thermal treatment. Based on TGA tests
438 results (no release event below 400°C), the I_2 release kinetics was monitored from $\sim 330^\circ\text{C}$ on.

439 A first test has been performed in an argon/steam atmosphere (condition 5), serving as reference
440 (Figure 3, red curve). There is no signal increase up to 640°C, indicating the lack of gaseous I_2 . The
441 weak signal detected in the 640-680°C temperature range and interpreted as $N_{rel} \neq 0$ is nevertheless
442 not representative of any I_2 release kinetics. Indeed, the raw spectra in this temperature range lack
443 the fine structure of the I_2 spectrum [38] [34] and thus the signal is attributed to the light extinction
444 due to the presence of aerosols (probably CsI) transported up to the optical cell. This online
445 measurement experiment with a sensitive technique confirmed the absence of gaseous molecular
446 iodine released in steam conditions.

447 In pure air (Table 2, condition 1), I_2 release starts at approx. 440°C, which is coherent with the TGA
448 tests, and occurs in two steps (Figure 3, blue curve):

- 449 1) Between ≈ 440 -550°C a first slow and low release is observed ;
- 450 2) Above 550°C the majority of iodine is rapidly released (exponentially). Reproducibility tests
451 have been performed in these conditions and the results were similar.

452 Further on, the re-vaporization tests in air/steam atmosphere (Table 2, conditions 2, 3 and 4) showed
453 that I_2 release is initiated at a higher temperature, ≈ 480 -500°C (Figure 4), compared to air re-
454 vaporization, which is coherent to the TGA results of similar tests. While the release of I_2 in two steps
455 is still noticeable for the % vol. 50/50 (condition 2), it is less pronounced for the other two carrier gas
456 compositions (conditions 3 and 4). It is also interesting to note that the release curves present
457 "spikes" (above $\approx 520^\circ\text{C}$), which resemble those in the case of argon/steam re-vaporization. This
458 suggests the presence of a larger amount of aerosols, which in turn prevent a reliable measurement
459 of I_2 .

460

461

462

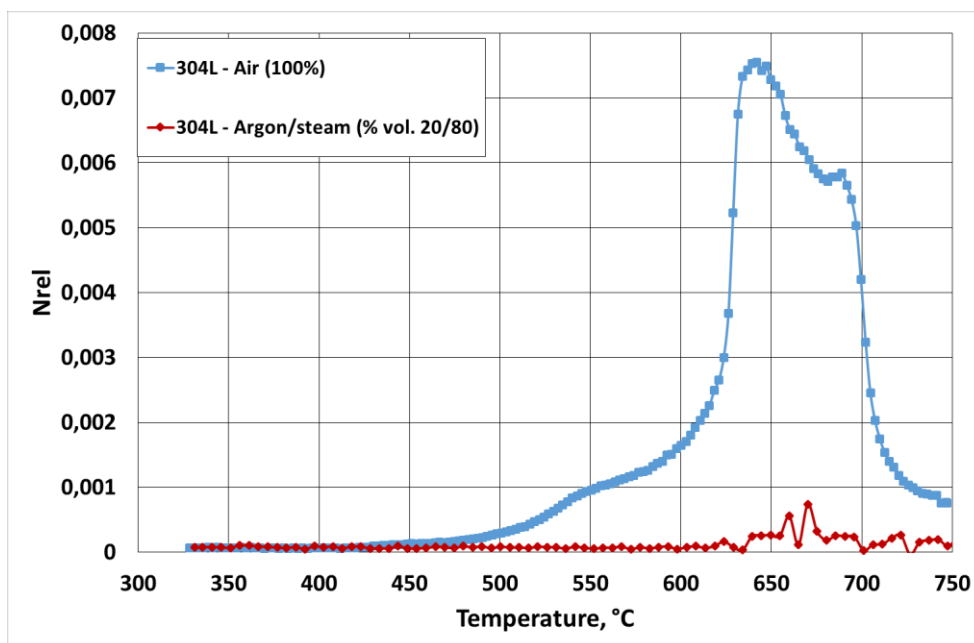
Table 3. Summary table of main experimental results.

Substrate	CsI deposit	Re-vaporization carrier gas (% vol)	Main results					Cond n°
			Temp. of release initiation (°C) ⁴	I ₂ released ^{1,2}	Cs residual ^{1,3}	I residual ^{1,3}	Cs/I line1	
Pre-oxidized 304L	Aerosols impaction at room temperature	Air (100%)	420	50-75 %	<10%	<1%	5-11	1
		Air/steam (50/50)	460	26%	6.5%	< l.d.	1.5	2
		Air/steam (20/80)	470	23-33%	7-9%	< l.d.	1.6	3
		Air/steam (3/97)	450	26%	2%	< l.d.	1.4	4
		Argon/steam (70/30)	480	0%	3.4%	< l.d.	1.1	5[29]
Pre-oxidized 316L	High-temperature vapour deposition (720-620°C)	Air (100%)		53%	3.4%	< l.d.	10	6
		Air/steam (20/80)		13%	9.7%	8.6%	1.6	7
		Argon/steam (70/30)		0%	1.9%	< l.d.	3.8	8
	Vapour condensation (620-440°C)	Air (100%)		7-15%	2.4-4.5%	<1%	1.3	9
		Air/steam (20/80)		12%	2.0%	<1%	1.1	10
		Argon/steam (70/30)		0%	0.5%	0.6%	3.1	11
	Aerosols deposits (< 400°C)	Air (100%)		45%	2.4%	< l.d.	12	12
		Argon/steam (70/30)		0%	2.9%	1.0%	1.2	13
	Gold (Au)	Aerosols Impaction (RT)	Air (100%)		28%	0.4%	< l.d.	1.6

463

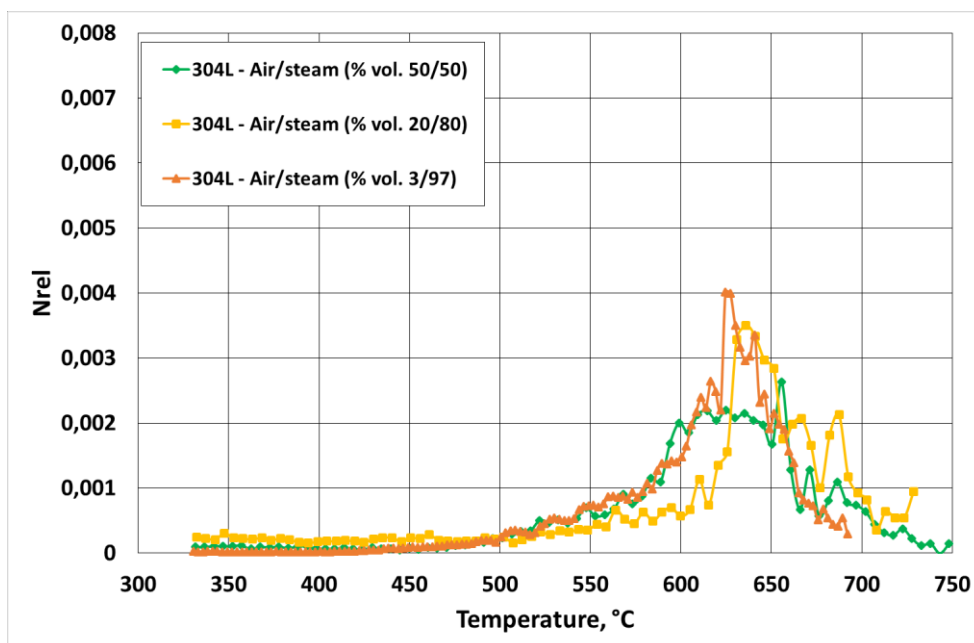
464
465
466

¹wt% wrt the total collected Cs and I at the end of test
³As measured by ICP-MS
²As measured by UV-Visible spectroscopy
⁴As measured by TGA



467
468

469 Figure 3. Release and transport kinetics of I₂ during re-vaporization of CsI aerosols (RT aerosol impaction) with a heating
470 rate of 5°C/min up to 750°C; blue curve : pure air with a flow rate of 53 mL_n/min (condition 1) ; red curve : argon/steam
471 (70/30) with flow rate of 200 mL_n/min (condition 5).



472
473
474
475

473 Figure 4. Release and transport kinetics of I₂ during re-vaporization of CsI aerosols (RT aerosol impaction) with a heating
474 rate of 5°C/min up to 750°C. green curve: air/steam % vol. 50/50 (condition 2); yellow curve ; air/steam % vol. 20/80
475 (condition 3); orange curve : air/steam % vol. 3/97 (condition 4). Gas flow: 200 mL_n/min for all conditions.

476 **4.2.2. Influence of CsI deposition process: high-temperature (conditions 6-13) vs. aerosol**
477 **impaction at room temperature**

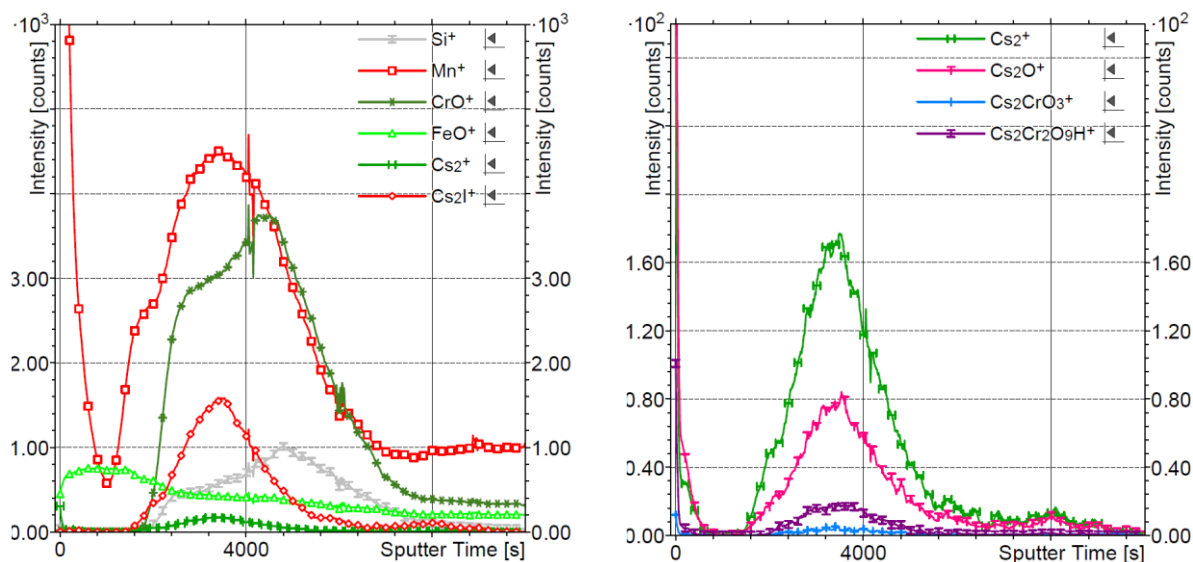
478 As a general rule, the re-vaporization of CsI deposits obtained by different routes follows the same
479 trend if the same experimental conditions are applied.

480 Compared to RT aerosol impaction, CsI aerosols deposited in the 400-150°C temperature range
481 present a similar re-vaporization behaviour with atmosphere composition (table 3, air and
482 argon/steam conditions only): similar gaseous iodine releases and overall deposition trends were
483 observed for the RIGolo integral tests. It is thus assumed that CsI re-vaporization behaviour is very
484 close when considering deposited aerosols.

485 For the two other deposition routes (high temperature vapour deposition 720-620°C and vapour
486 condensation 620-440°C), re-vaporization in argon/steam (conditions 8 and 11) didn't lead to the
487 release of I₂; those results are comparable to the re-vaporization of CsI aerosols (conditions 5 and
488 12). Nevertheless, the Cs/I mass ratio in the RIGolo line is much higher (3.8 and 3.1 for conditions 8
489 and 11 respectively) compared to condition 5 (1.1). This observation indicates that besides CsI, other
490 species can be involved during steam re-vaporization of such CsI deposits. CsOH is a possible
491 candidate for the other Cs compounds, the iodine transported species could not be clearly identified.

492 Re-vaporization in air of the high-temperature deposits (condition n°6) and the aerosols deposits in
493 has resulted in the release of 53% of iodine as I₂. The ICP-MS analysis of the alumina tube leachate
494 shows a Cs/I mass ratio ~ 10. Both results are consistent with the re-vaporization behaviour of CsI
495 aerosols as described in section 4.2.1. Only one mixed air/steam carrier gas composition (% vol.
496 20/80) was tested with the high-temperature (720-620°C, condition 7) and vapour condensation
497 (620-440°C, condition 10) deposits. The results show that 12-13% of iodine is released as I₂ and that
498 the Cs/I ≈ 1.1 – 1.6 in the alumina tube, which is again consistent with the results presented in
499 section 4.2.1. However, there was a noticeable difference in the amount of released molecular iodine
500 for condition 9. The re-vaporization in pure air of a CsI deposit obtained by vapour condensation
501 (620-440°C) resulted in the release of only 7-15% of I₂, which is much lower when compared to the
502 amount of released I₂ in other experiments in the same re-vaporization conditions. The residual
503 amount of Cs on the steel coupon is 2.4 – 4.5 % and the Cs/I ≈ 1.3 in the alumina tube, suggesting the
504 re-vaporization of Cs as several different species. The possible reasons, which may be linked to the
505 organized crystalline structure of the deposit, are discussed further.

506 Surface characterizations by XPS and ToF-SIMS have been performed on the 316L foils after CsI re-
507 vaporization of high temperature deposits and condensed vapour (as displayed in figure 6). The
508 presence of the mixed Cs-Cr-O compounds described above (see section 4.2.1) is confirmed (figure
509 6b, depth profiles in negative polarity), as soon as air is present in the carrier gas. Also, in both cases,
510 the Cs depth profile indicates that Cs had migrated in the oxide layer during the thermal treatment –
511 or that the oxide layer may have growth up to the CsI deposit. Indeed the Cs₂⁺ and Cs₂I⁺ signals are
512 very low at the surface and in the first oxide layer (composed of Fe and Mn) and increase strongly in
513 the second Cr-Mn oxide layer (figure 6, depth profile in positive polarity). Migration of CsI inside the
514 oxide layer may explain the significantly more important residual mass of Cs (9.7%) and I (8.6%)
515 observed on the 316L foil after re-vaporization of high-temperature vapour deposit in steam/air
516 (table 3, condition 7) .



517

518

519

Figure 5. TOF-SIMS profile of CsI vapour condensation deposition 316L pre-oxidized foil and re-vaporized in air/steam atmosphere (condition 10, table 3). Secondary ions in positive polarity a) major fragments and b) minor fragments.

520

521

522

523

524

525

526

Based on the results of the integral tests, online measurement tests have been performed with CsI high-temperature (720-620°C) and vapour condensation (620-440°C) deposits with the same thermal cycle as for conditions 6 and 9. The carrier gas was pure air. The I₂ release kinetics from CsI deposits obtained by vapour condensation (condition n°9) presents a similar pattern as from CsI deposits obtained by RT aerosol impaction (condition n°1) (Figure 6). The process occurred in two steps: 1) a slow and low release between ≈350-500°C, and 2) a more rapid re-vaporization above 500°C, which results in the total release of iodine from the surface of the pre-oxidized 316L foil.

527

528

529

530

531

532

533

534

535

536

537

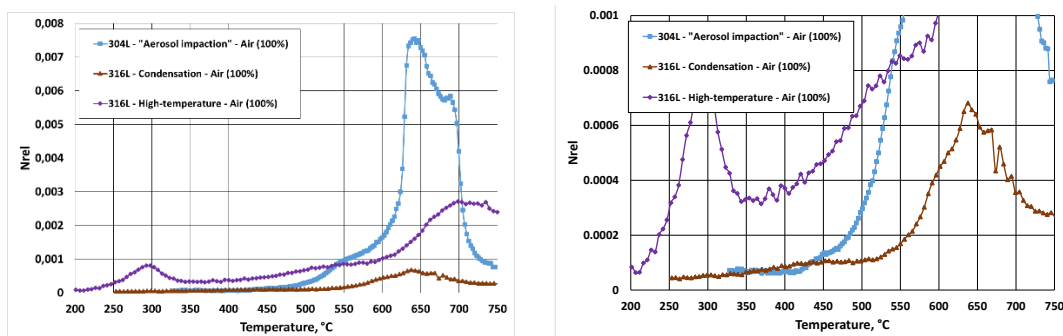
538

The kinetic study of I₂ release in case of a high-temperature CsI deposit (720-620°C), on the contrary, has highlighted a new phenomenon. While the cumulated amount of released I₂ is consistent with the release observed in condition 1 (RT aerosol impaction), the I₂ release and transport kinetics is slightly different (Figure 5). There is a two-step molecular iodine release between ≈400-550°C (slow) and above 550°C (rapid), which is consistent with previous results. However, there is an additional release peak between ≈200-350°C, which has been reproduced in another test, hinting at a different re-vaporization process, probably linked to the nature of the deposit in this temperature range (720-620°C). This new release mechanism may be owed to the CsI deposition temperature which resulted in a non-uniform amorphous like layer of deposits (see section 4.1) which is quite different to aerosol impaction [29] so that one can expect strong evolution at the molecular level too (for instance in the structure of the CsI outermost surface), inducing differences in the reaction mechanism – as will be seen with the DFT calculations (section 5).

539

540

The kinetic test results have shown the absence of any release below 200°C, hence the I₂ release kinetics for this series of tests is shown starting at ≈170-250°C.



541

542 **Figure 6. Release and transport kinetics of I₂ during re-vaporization of CsI deposits in pure air with a heating rate of**
 543 **5°C/min up to 750°C; blue curve : CsI RT aerosol impaction" (condition 1, air flow rate 53 mL_n/min), brown curve: CsI**
 544 **vapour condensation (condition 9, air flow rate 200 mL_n/min); purple curve : CsI high-temperature vapour deposition**
 545 **(condition 6, air flow 200 mL_n/min)**

546 **4.2.3. Influence of substrate nature: stainless steel vs. gold inert surface (condition 14)**

547 A previous study [49] has linked the formation of gaseous molecular iodine to the interaction
 548 between CsI and Cr₂O₃ in presence of dioxygen. This assumption is supported by the fact that the
 549 reaction cited by Sasaki *et al.* [49] is thermodynamically favoured in the temperature range of our
 550 conditions. In air conditions, our observations (release of I₂ and formation of caesium chromate
 551 species) allowed us to propose a similar reactivity with the surface [31]. For the further
 552 understanding of the phenomenon, it was decided to perform additional tests whose goals were to
 553 determine whether there are other mechanisms involved in the formation of I₂, besides CsI-substrate
 554 interaction.

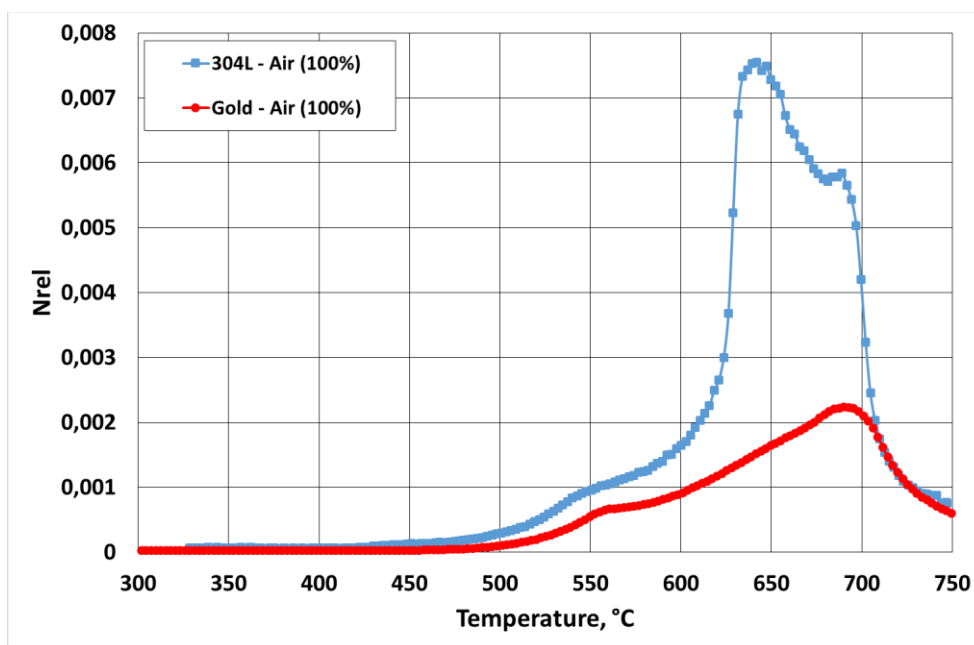
555 Consequently, CsI aerosol deposits (aerosol impaction at room temperature) have been generated
 556 on a chemically inert surface – gold coupons, and a series of re-vaporization tests in pure air have
 557 been performed afterwards (condition n°14). Integral tests in the RIGolo device have led to the total
 558 release of caesium (0.4% detected on the coupon after re-vaporization by ICP-MS) and iodine from
 559 the surface of the gold coupon. The Cs/I ≈ 1.6 in the alumina tube, suggesting again the re-
 560 vaporization of Cs under other species besides CsI compounds. Up to 28% of iodine has been
 561 released as I₂ (relative to the total measured amount of iodine at the end of test), which is lower
 562 compared to the re-vaporization from the pre-oxidized 304L coupons and 316L foils in the same
 563 conditions (conditions 1 and 12 respectively). Nevertheless, this lower release may be owed to
 564 deposit inhomogeneities. These results suggest that the formation of I₂ is not due only to the
 565 interaction of CsI with the oxide substrate, but that the oxidation of iodide by the gas phase plays an
 566 important role in iodine vaporization.

567 From a kinetic point of view, TGA analysis has shown that the process is initiated at a higher
 568 temperature (526°C) compared to CsI re-vaporization onset on 304L coupons (see section 4.2.1).
 569 Figure 7 shows the gaseous molecular iodine release kinetics and the pattern clearly resembles that
 570 of CsI re-vaporization from pre-oxidized stainless steel surface (condition n°1):

- 571 1) A low release between ≈450-560°C;
- 572 2) A more important release (up to the depletion of the iodine source) above 560°C. It is worth
 573 noting that this release is slower compared to the release in condition n°1.

574 This suggests that the mechanisms governing the formation of I_2 are very close, regardless of the
575 substrate. As a consequence, the role of pre-oxidized stainless steel in the production of gaseous
576 iodine species is less important than initially expected.

577 Nevertheless, the differences observed between kinetic of I_2 productions when considering an inert
578 surface and pre-oxidized stainless steel, indicates that some substrate effect cannot be excluded at
579 high temperature.



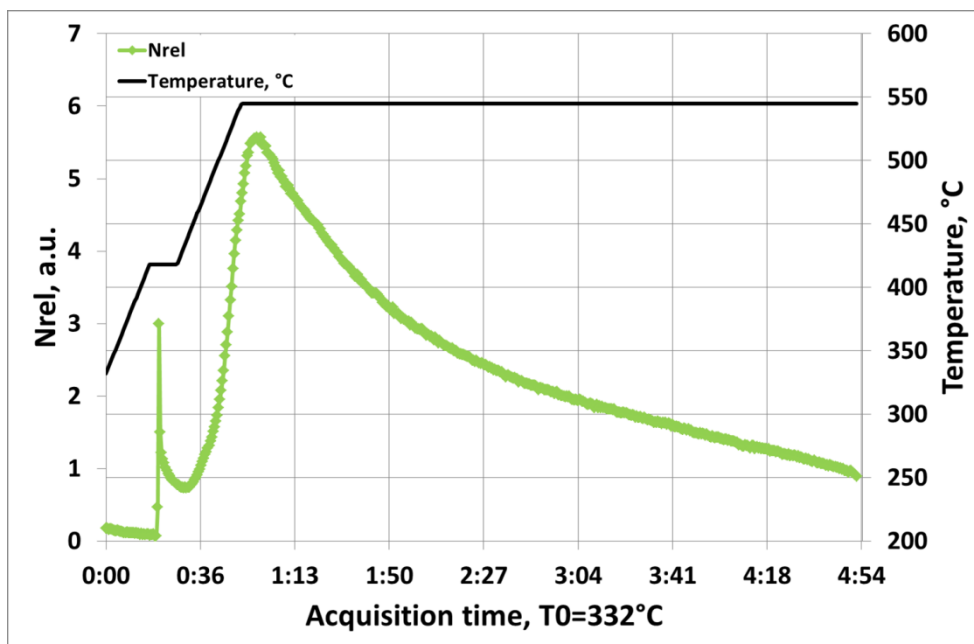
580
581 **Figure 7. Release and transport kinetics of I_2 during re-vaporization of CsI aerosols (RT aerosol impaction) in pure air (53**
582 **53 mLn/min) and with a heating rate of 5°C/min up to 750°C; blue curve: pre-oxidized 304L surface ; red curve : gold**
583 **surface.**

584 4.2.4. Thermal cycle boundaries : kinetic of I_2 release up to 550°C

585 Based on the results of previous online measurement tests, it was decided to conduct another one
586 with a limited maximum temperature of $\approx 550^\circ\text{C}$, which is the upper limit for the first step of I_2
587 release. The goal was to study the release phenomenon in the 450-550°C range. In order to reduce
588 the carrier gas interference at low temperature, the sample was heated under argon up to $\approx 420^\circ\text{C}$,
589 and then the carrier gas was switched to a mixture of air/steam (% vol. 50/50). Figure 7 shows the I_2
590 release and transport kinetics and it can be noticed that the release starts at $\approx 440^\circ\text{C}$ and ends just
591 after the final temperature of $\approx 550^\circ\text{C}$ is reached, with a subsequent decrease in signal, which is
592 probably due to the depletion of the source involved in this first mechanism. The fine peak at 420°C
593 is an artifact in the IBBCEAS response due to a transient overpressure in the IBB CEAS cell when
594 switching the carrier gas composition from argon to the air/steam mix. This transient induced a shift
595 in the baseline which could not be corrected during the test. The I_2 spectral fingerprint is indeed
596 clearly observed from 450°C on.

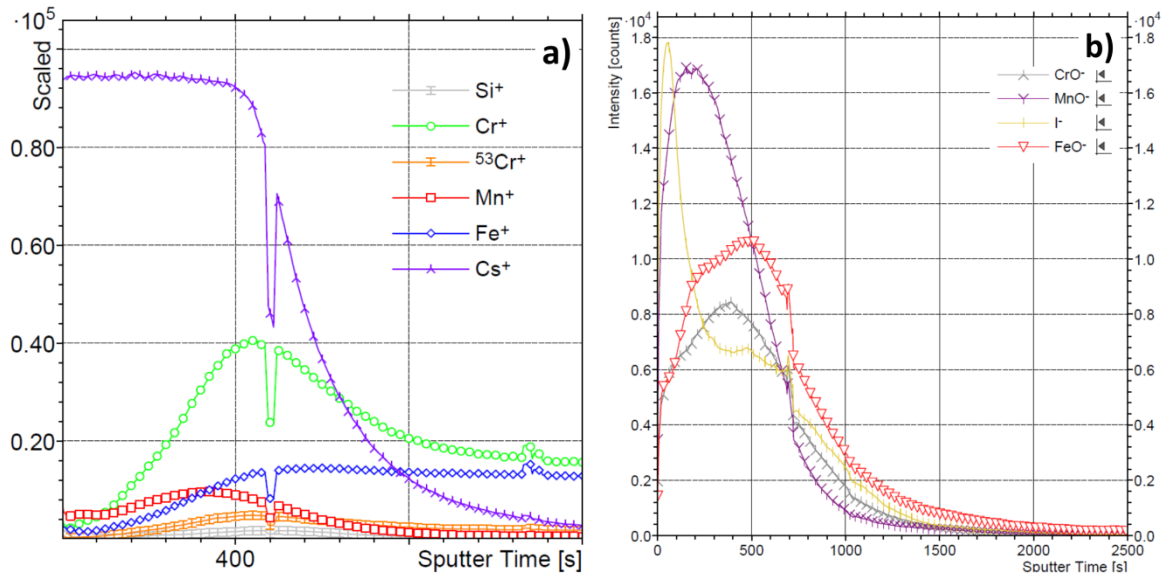
597 No integral test in the RIGolo device has been performed in these conditions, but surface
598 characterization by ToF-SIMS of the sample has been done. The depth profile analysis in positive
599 polarity revealed an intense Cs^+ signal (Figure 8a), while the analysis in negative polarity has revealed
600 the presence of relatively intense I^- secondary ions (Figure 8b). Also, the secondary ion clusters

601 $\text{Cs}_2\text{CrO}_3^+$ and $\text{Cs}_2\text{Cr}_2\text{O}_9\text{H}^+$ have been detected, which indicates the formation of Cs-Cr-O compounds.
 602 All these results suggest that a part of iodine has been released from the surface as I_2 and that
 603 caesium mainly remained on the surface, both as CsI and mixed Cs-Cr oxides. Furthermore, it would
 604 seem that up to 550°C the formation of I_2 is based on the reaction between the CsI deposit and
 605 carrier gas components in a heterogeneous phase. The most intense release observed above 550°C
 606 (Figure 3, blue curve) could then be explained by the vaporization of CsI deposits (which starts
 607 between 550 and 600°C) followed by a reaction in gaseous (homogeneous) phase, which would
 608 favour the contact between CsI and carrier gas molecules. In this latter case, the residual quantity of
 609 Cs on the surface would be low as observed in condition 1 (see table 3).



610

611 **Figure 8. Release and transport kinetics of I_2 during re-vaporization of CsI aerosols (RT aerosol impaction) from pre-**
 612 **oxidized 304L coupon. Thermal cycle and carrier gas composition: 1) heating up to 420°C in argon; 2) maintain for 10 min**
 613 **at 420°C , switching to air/steam (% vol. 50/50); 3) heating up to 550°C and 4) maintain at 550°C for 6h. Gas flow**
 614 **$200\text{mL}_n/\text{min}$. Heating up at $5^\circ\text{C}/\text{min}$.**



615

616
617

Figure 9. ToF-SIMS depth profile of a CsI aerosol deposit re-vaporized from pre-oxidized 304L coupon: a) secondary ions in positive polarity and b) secondary ions in negative polarity.

618

5. Theoretical modelling

619

620

621

622

623

624

625

626

627

628

629

630

631

632

633

5.1. Model

634

635

636

637

638

639

640

641

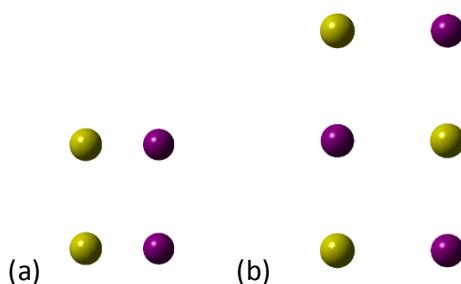
CsI crystal has a simple cubic structure which belongs to the Pm3m group, with two atoms in the unit cell, caesium at (0, 0, 0) and iodine at (a/2) (1, 1, 1) while 'a' being the lattice constant (456.67 pm)[50] kept fixed in the calculation at the experimental. The nature of the exposed surface is defined by the surface energy of low index surfaces. In order to compute them, we define super-cell composed of at least 8 layer of CsI and added 15 Å of vacuum to avoid any interaction between the slab. The four outermost layers have been relaxed. The surface energies of low index surfaces are summarized in table 4.

Table 4 : Surface energy (mJ.m⁻²) after relaxation of low index surfaces.

Surface index	(011)	(111)	(210)	(211)	(001)
Surface energy (mJ.m ⁻²)	193	520	365	417	615

642

643 The (011) surface is the most stable one and considering the large surface energy difference, it will
644 be the only surface exposed by dehydrated CsI particles. The (011) surface is composed of alternating
645 rows of Cs and I anions.
646

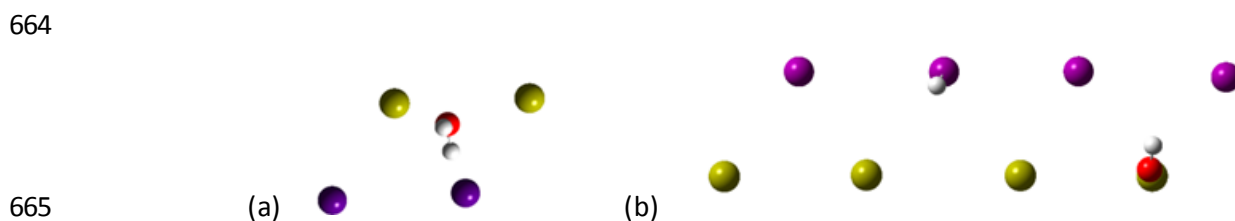


647
648 **Figure 10. Top (a) and side (b) view of the (011) surface (most stable surface)(Cs in yellow, I in purple).**

649 **5.2. H₂O and O₂ Interaction with perfect (011) surfaces.**

651
652 The reactive molecules in the gas phase during the experiments are water and dioxygen. We studied
653 theoretically the interaction of these two molecules with the CsI surfaces to determine the reaction
654 that may occur on the surface and may explain the iodine revaporisation.

655
656 The water adsorption on the surface is molecular. One hydrogen atom of the water molecule forms a
657 hydrogen bond with the surface iodine while the negatively charged oxygen atom interacts with the
658 Cs cation. The Cs-O and H-I distances are 3.16 and 2.45 Å respectively. The adsorption energy is 0.52
659 eV. The adsorption is exothermic but as the main interaction is a weak hydrogen bond, the water
660 molecule adsorption will not be favoured at high temperature. We tested the dissociative adsorption
661 of the water molecule on the surface to form both Cs-OH and HI groups. This adsorption is very
662 endothermic (-3,54 eV). The formation of IH groups on the perfect surface is not possible and such
663 we can exclude the departure of HI(g) molecule from the surface.



665
666 **Figure 11. Water adsorption on the perfect (011) surface (a) molecular adsorption (b) dissociative adsorption**
667 **(Cs in yellow, I in purple, O in red, H in white).**

668
669 The oxygen molecule adsorption on the surface is also a molecular one. The O₂ molecule is located in
670 a η² geometry, on top of one Cs cation. The O-Cs distances are 3.04 Å and the O-O one is 1.24 very
671 close to the O-O distance in the gas phase (. The adsorption is endothermic (E_{ads} = -0.18 eV). We
672 study the dissociative adsorption. The oxygen atoms are located in the first surface plane, between
673 Cs and I ion. This adsorption mode is even more endothermic (E_{ads}= -0.88 eV) than the molecular
674 one. The oxygen adsorption and reaction with a perfect surface is not probable at high temperature.

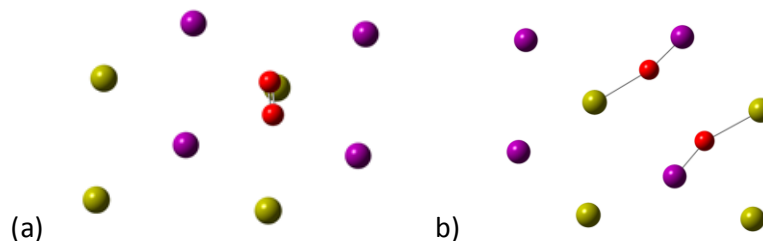


Figure 12. O₂ adsorption on the perfect (011) surface (a) molecular adsorption (b) dissociative adsorption (Cs in yellow, I in purple, O in red).

5.3. O₂ interaction with defective surfaces.

The presence of defects on the surface increases their reactivity. To model these defects, we study the O₂ interaction with a step (011) surface: i.e. the (014) surface, composed a step and a (011) terrace (figure 13). The iodine ions located on the step are under-coordinated which would increase their reactivity.

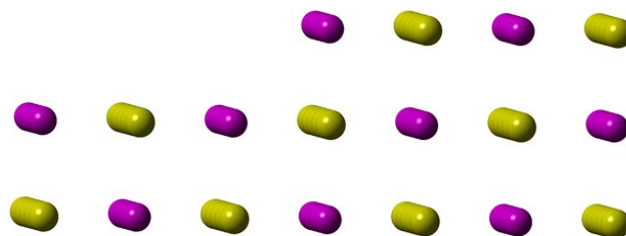


Figure 13. Side view of the stepped (014) surface (Cs in yellow, I in purple).

On the opposite to the perfect surface, the oxygen molecular adsorption on the iodine ion located on the step is an exothermic process ($\Delta E = -0,57 \text{ eV}/E_{\text{ads}} = 0,57 \text{ eV}$) (b step, figure 14) . The oxygen molecule is located between two iodine anions of the edge. The I-O distance is $2,86 \text{ \AA}$ and the O-O one is $1,27 \text{ \AA}$, $0,04 \text{ \AA}$ larger than the distance for the gas phase molecule. The oxygen molecule is activated when adsorbed on a defect. The dissociative adsorption is favoured on the edge. The adsorption energy is then $1,07 \text{ eV}$ (c step, figure 14) . One the oxygen molecule is dissociated on the surface, the desorption of IO^\bullet radical is possible. This final step is endothermic (d step , figure 14) but will be favoured by a very concentration of iodine in the gas and by the continuous gas flow above the surface. IO^\bullet being a strong oxidant it will react with the iodide to produce $\text{I}_{2(\text{g})}$ as demonstrated in liquid [51] and in the gas phase[52].

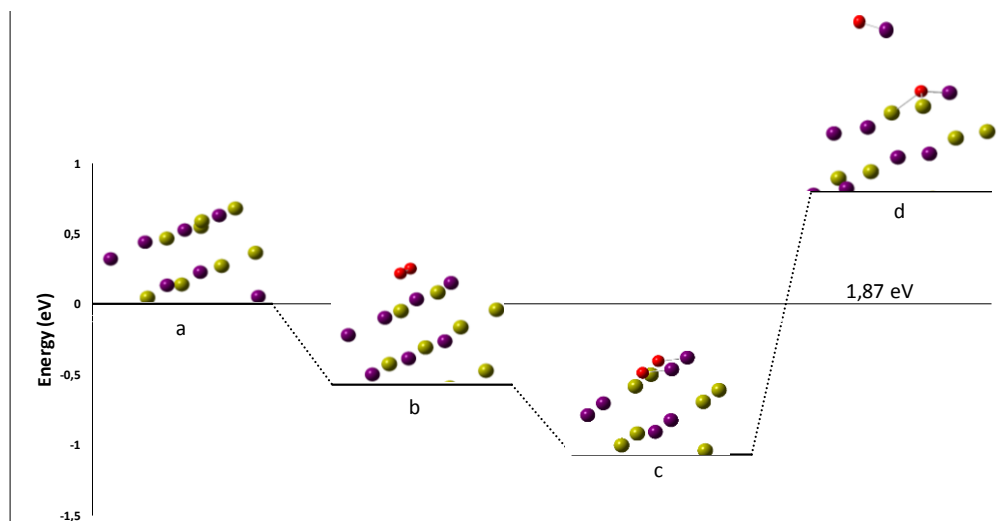


Figure 14. Adsorption and dissociation of O₂ on stepped surface (Cs in yellow, I in purple, O in red).

700
701
702
703
704
705
706
707

In order to get insight in the kinetic of the oxygen molecule dissociation on the surface, we computed the activation energy of the reaction (figure 15). The activation energy is small ($E_{act} = 0,64$ eV), which indicate that the surface oxidation will be fast on defects. The O-O distance on the transition state is 1.77 Å.

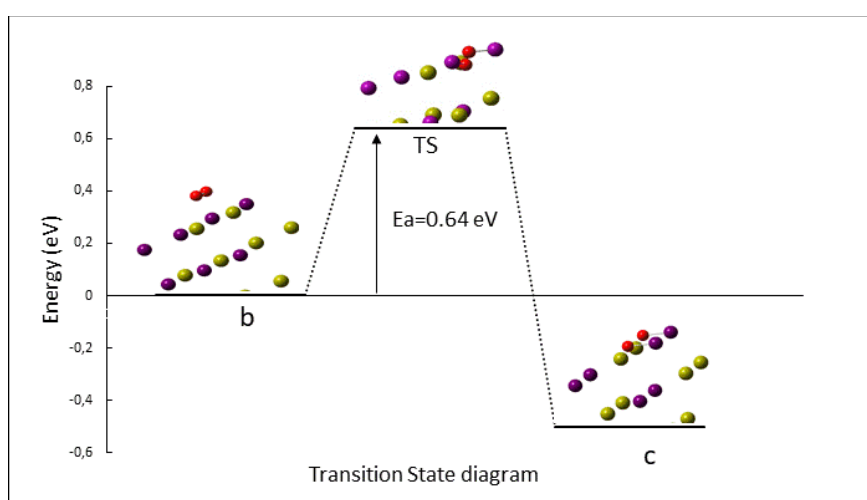


Figure 15. O₂ activation mechanism on the step surface ((Cs in yellow, I in purple, O in red).

708
709
710
711
712
713
714
715
716
717
718
719
720
721

From the DFT calculation, we can conclude that the water molecule will not be involved directly in the CsI oxidation reactions and in the I₂ formation. However, when the quantity of water in the feed is much larger than the oxygen one, the water will have a competitive adsorption on the surface.

On the opposite to water, the O₂ molecules can react on the CsI particles to form in the first step the radical species IO[•], but this process will mainly occur on the surface defects. The oxygen reactivity depends then of the nature of the surface and on the numbers of defects. However, once the IO[•] radical have been formed, this reactive species may react with the surface and such create defects on the particle surface. This mechanism may be responsible for the very fast increase of the reaction rate with temperature that is observed experimentally. It may be mentioned that the CsI reactivity at low temperature (around 400° C according to the experiments) will depend on the exact nature of the surface and on the

722 deposition method. A fast cooling of hot particles on the surface will favour the formation of
723 defects and increased its reactivity.

724
725
726

6. Conclusion

727 From the experimental study, the following trends can be summarized as follows:

- 728 - In presence of air, the re-vaporization of CsI deposits from pre-oxidized stainless steel
729 surfaces leads to the release of 45-75% of I₂ from initial iodine inventory – except for CsI
730 deposit by vapour condensation. A part of Cs is retained on the surface (2.5-10% of initial
731 amount) and forms mixed Cs-Cr-O compounds;
- 732 - In a mixed air/steam atmosphere, between 12-33% of iodine is released as I₂, regardless of
733 the air content in the carrier gas, the molecular iodine fraction probably depends on air
734 content and temperature deposits ;
- 735 - The deposit nature (aerosol, high temperature vapour deposition and vapour condensation)
736 does not seem to influence the amount of released molecular iodine strongly or retained
737 caesium. An exception is the CsI deposit by vapour condensation (620-440°C) which is
738 crystalline and thus has an organized structure;
- 739 - The re-vaporization of CsI aerosols from an inert surface (gold) in air leads to the formation
740 of 28% of molecular iodine (relative to I initial amount), which is lower compared to the re-
741 vaporization from a stainless steel surface;
- 742 - The gaseous molecular iodine release kinetic pattern is generally the same, regardless of
743 carrier gas composition, deposit or substrate nature and consists of two steps: an initial
744 reduced release between ≈440-550°C and a second rapid release above 550°C. In the case of
745 CsI high-temperature deposits (720-620°C) there is an additional I₂ release peak between
746 200-350°C.

747 The analysis of these results allows us to make the following conclusions and hypotheses:

- 748 - There seem to be several mechanisms responsible for I₂ formation, depending on the
749 temperature. Below 550°C the results suggest a solid-gas (heterogeneous) phase interaction
750 between the deposit and the carrier gas. Above 550°C, the CsI starts to vaporize and the
751 interaction is in gas (homogeneous) phase, which would explain the increased rate of I₂
752 release;
- 753 - The iodine formation is favoured on the CsI surface defects, and such is influenced by the CsI
754 deposition process. The I₂ formation start at higher temperature on well crystallized
755 particles. However, the formation of the first I₂ molecules will induce the formation of
756 defects on the surface which will increase the surface oxidation rate.

757 To develop some models and cover severe accident boundary conditions, additional experimental
758 investigations are needed to explore other fission products and other gas composition.

759

760 Acknowledgements

761 This work was performed in the frame of the French research program ANR-11-RSNR-0013-01 called
762 MiRE (Mitigation of outside releases in case of nuclear accident), with the financial support of EDF
763 and Framatome. The authors thank the HPC centre of the Lille University for providing CPU
764 resources. Surface analysis have been performed at the 'plateforme d'analyses de surfaces' of the
765 Lille University.

766

767

769 References

- 770 1. Cantrel L, Cousin F, Bosland L, et al (2014) ASTEC V2 severe accident integral code: Fission
771 product modelling and validation. *Nuclear Engineering and Design* 272:195–206.
772 <https://doi.org/10.1016/j.nucengdes.2014.01.011>
- 773 2. Haste T, Payot F, Bottomley PDW (2013) Transport and deposition in the Phébus FP circuit.
774 *Annals of Nuclear Energy* 61:102–121. <https://doi.org/10.1016/j.anucene.2012.10.032>
- 775 3. Cantrel L, Albiol T, Bosland L, et al (2018) Research Works on Iodine and Ruthenium Behavior in
776 Severe Accident Conditions. *Journal of Nuclear Engineering and Radiation Science* 4:020903.
777 <https://doi.org/10.1115/1.4038223>
- 778 4. Hidaka A, Igarashi M, Hashimoto K, et al (1995) Experimental and Analytical Study on the
779 Behavior of Cesium Iodide Aerosol/Vapor Deposition onto Inner Surface of Pipe Wall under
780 Severe Accident Conditions. *Journal of Nuclear Science and Technology* 32:1047–1053.
781 <https://doi.org/10.1080/18811248.1995.9731813>
- 782 5. Maruyama Y, Shibasaki H, Igarashi M, et al (1999) Vapor Condensation and Thermophoretic
783 Aerosol Deposition of Cesium Iodide in Horizontal Thermal Gradient Pipes. *Journal of Nuclear
784 Science and Technology* 36:433–442. <https://doi.org/10.1080/18811248.1999.9726226>
- 785 6. Girault N, Payot F (2013) Insights into iodine behaviour and speciation in the Phébus primary
786 circuit. *Annals of Nuclear Energy* 61:143–156. <https://doi.org/10.1016/j.anucene.2013.03.038>
- 787 7. Katata G, Chino M, Kobayashi T, et al (2015) Detailed source term estimation of the
788 atmospheric release for the Fukushima Daiichi Nuclear Power Station accident by coupling
789 simulations of an atmospheric dispersion model with an improved deposition scheme and
790 oceanic dispersion model. *Atmospheric Chemistry and Physics* 15:1029–1070.
791 <https://doi.org/10.5194/acp-15-1029-2015>
- 792 8. Terada H, Katata G, Chino M, Nagai H (2012) Atmospheric discharge and dispersion of
793 radionuclides during the Fukushima Dai-ichi Nuclear Power Plant accident. Part II: verification
794 of the source term and analysis of regional-scale atmospheric dispersion. *Journal of
795 Environmental Radioactivity* 112:141–154. <https://doi.org/10.1016/j.jenvrad.2012.05.023>
- 796 9. Anderson, A., Auvinen, A., Bottomley, P., Bryan, C., Freemantle, N., Hieraut, J., Jokiniemi, J.,
797 Kingsbury, A., & Tuson, A. (2000). Revaporisation tests on samples from Phebus fission
798 products: Final report. (Issue 2 ed.) AEA Technology Report, No. AEAT/R/NS/0124
- 799 10. Auvinen A, Lehtinen KEJ, Enriquez J, et al (2000) VAPORISATION RATES OF CsOH AND CsI IN
800 CONDITIONS SIMULATING A SEVERE NUCLEAR ACCIDENT. *Journal of Aerosol Science* 31:1029–
801 1043. [https://doi.org/10.1016/S0021-8502\(00\)00027-6](https://doi.org/10.1016/S0021-8502(00)00027-6)
- 802 11. Bottomley PDW, Knebel K, Van Winckel S, et al (2014) Revaporisation of fission product
803 deposits in the primary circuit and its impact on accident source term. *Annals of Nuclear Energy*
804 74:208–223. <https://doi.org/10.1016/j.anucene.2014.05.011>
- 805 12. Knebel K, Bottomley PDW, Rondinella VV, et al (2014) An experimental device to study the
806 revaporisation behaviour of fission product deposits under severe accident conditions. *Progress
807 in Nuclear Energy* 72:77–82. <https://doi.org/10.1016/j.pnucene.2013.07.022>

- 808 13. Kalilainen J, Kärkelä T, Zilliacus R, et al (2014) Chemical reactions of fission product deposits and
809 iodine transport in primary circuit conditions. Nuclear Engineering and Design 267:140–147.
810 <https://doi.org/10.1016/j.nucengdes.2013.11.078>
- 811 14. Shibazaki H, Maruyama Y, Kudo T, et al (2001) Revaporization of a CsI Aerosol in a Horizontal
812 Straight Pipe in a Severe Accident Condition. Nuclear Technology 134:62–70.
813 <https://doi.org/10.13182/NT01-A3186>
- 814 15. Berdonosov s. s., Sitova m. a. (1997) Chemical Forms of Iodine Occurring at Evaporation and
815 Condensation of Cesium Iodide in Air. Radiochemistry 39:341–342
- 816 16. Berdonosov s. s., Baronov s. b. (1999) Interaction of caesium Iodide with an Air Flow at High
817 Temperatures. Radiochemistry 41:63–66
- 818 17. Kulyukhin SA, Mikheev NB, Kamenskaya AN, et al (2004) Oxidative Hydrolysis in Water Vapor-
819 Air Phase of CsI Radioaerosols Produced by CsI Sublimation from Metallic Surface.
820 Radiochemistry 46:63–66. <https://doi.org/10.1023/B:RACH.0000024639.33411.68>
- 821 18. Hijazi H (2017) RÉACTIVITÉ CHIMIQUE DES AÉROSOLS D'IODE EN CONDITIONS ACCIDENTELLES
822 DANS UN RÉACTEUR NUCLÉAIRE. Université de Lille
- 823 19. Khanniche S, Louis F, Cantrel L, Černušák I (2017) Investigation of the Reaction Mechanism and
824 Kinetics of Iodic Acid with OH Radical Using Quantum Chemistry. ACS Earth and Space
825 Chemistry 1:227–235. <https://doi.org/10.1021/acsearthspacechem.7b00038>
- 826 20. Khanniche S, Louis F, Cantrel L, Černušák I (2017) Thermochemistry of HIO₂ Species and
827 Reactivity of Iodous Acid with OH Radical: A Computational Study. ACS Earth and Space
828 Chemistry 1:39–49. <https://doi.org/10.1021/acsearthspacechem.6b00010>
- 829 21. Villard A, Khanniche S, Fortin C, et al (2019) A theoretical study of the microhydration processes
830 of iodine nitrogen oxides. International Journal of Quantum Chemistry 119:e25792.
831 <https://doi.org/10.1002/qua.25792>
- 832 22. Khiri D, Vandeputte R, Taamalli S, et al (2019) Microhydration of caesium metaborate:
833 structural and thermochemical properties of CsBO₂ + n H₂O (n = 1–4) aggregates. Journal of
834 Molecular Modeling 25:. <https://doi.org/10.1007/s00894-019-4094-4>
- 835 23. Khanniche S, Louis F, Cantrel L, Černušák I (2016) Computational study of the I₂O₅ + H₂O = 2
836 HOIO₂ gas-phase reaction. Chemical Physics Letters 662:114–119.
837 <https://doi.org/10.1016/j.cplett.2016.09.023>
- 838 24. Khanniche S, Louis F, Cantrel L, Černušák I (2016) A theoretical study of the microhydration of
839 iodic acid (HOIO₂). Computational and Theoretical Chemistry 1094:98–107.
840 <https://doi.org/10.1016/j.comptc.2016.09.010>
- 841 25. Khanniche S, Louis F, Cantrel L, Černušák I (2016) A Density Functional Theory and *ab Initio*
842 Investigation of the Oxidation Reaction of CO by IO Radicals. The Journal of Physical Chemistry
843 A 120:1737–1749. <https://doi.org/10.1021/acs.jpca.6b00047>
- 844 26. Sudolská M, Cantrel L, Budzák Š, Černušák I (2014) Molecular structures and thermodynamic
845 properties of monohydrated gaseous iodine compounds: Modelling for severe accident
846 simulation. Journal of Nuclear Materials 446:73–80.
847 <https://doi.org/10.1016/j.jnucmat.2013.11.029>

- 848 27. Sudolská M, Cantrel L, Černušák I (2014) Microhydration of caesium compounds: Cs, CsOH, Csl
849 and Cs₂I₂ complexes with one to three H₂O molecules of nuclear safety interest. *Journal of*
850 *Molecular Modeling* 20:. <https://doi.org/10.1007/s00894-014-2218-4>
- 851 28. Šulková K, Cantrel L, Louis F (2015) Gas-Phase Reactivity of Cesium-Containing Species by
852 Quantum Chemistry. *The Journal of Physical Chemistry A* 119:9373–9384.
853 <https://doi.org/10.1021/acs.jpca.5b05548>
- 854 29. Taamalli S, Khiri D, Suliman S, et al (2020) Unraveling the Tropospheric Microhydration
855 Processes of Iodous Acid HOIO. *ACS Earth and Space Chemistry* 4:92–100.
856 <https://doi.org/10.1021/acsearthspacechem.9b00257>
- 857 30. Giordano P, Auvinen A, Brillant G, et al (2010) Recent advances in understanding ruthenium
858 behaviour under air-ingress conditions during a PWR severe accident. *Progress in Nuclear*
859 *Energy* 52:109–119. <https://doi.org/10.1016/j.pnucene.2009.09.011>
- 860 31. Obada D., Gasnot L, Mamede A-S, Grégoire A-C (2017) Assessment of medium-term radioactive
861 releases in case of a severe nuclear accident on a Pressurized Water Reactor: experimental
862 study of fission products re-vaporization from deposits (Cs, I). In: *Proceedings of ICAPP 2017.*
863 *Atomic Energy Society of Japan, Fukui and Kyoto (Japan)*, p 17328
- 864 32. Mamede A-S, Nuns N, Cristol A-L, et al (2016) Multitechnique characterisation of 304L surface
865 states oxidized at high temperature in steam and air atmospheres. *Applied Surface Science*
866 369:510–519. <https://doi.org/10.1016/j.apsusc.2016.01.185>
- 867 33. Obada D, Mamede A-S, Nuns N, et al (2018) Combined ToF-SIMS and XPS characterization of
868 304L surface after interaction with caesium iodide under PWR severe accident conditions.
869 *Applied Surface Science* 459:23–31. <https://doi.org/10.1016/j.apsusc.2018.07.212>
- 870 34. Johansson O, Mutelle H, Parker AE, et al (2014) Quantitative IBBCEAS measurements of I₂ in
871 the presence of aerosols. *Applied Physics B* 114:421–432. [https://doi.org/10.1007/s00340-013-](https://doi.org/10.1007/s00340-013-5536-9)
872 [5536-9](https://doi.org/10.1007/s00340-013-5536-9)
- 873 35. Obada D (2017) Evaluation de rejets moyen-terme en situation accidentelle grave d'un
874 Réacteur à Eau Pressurisée : étude expérimentale de la re-vaporisation de dépôts de produits
875 de fission (Cs, I). Université de Lille
- 876 36. Gouello M, Mutelle H, Cousin F, et al (2013) Analysis of the iodine gas phase produced by
877 interaction of Csl and MoO₃ vapours in flowing steam. *Nuclear Engineering and Design*
878 263:462–472. <https://doi.org/10.1016/j.nucengdes.2013.06.016>
- 879 37. Grégoire A-C, Kalilainen J, Cousin F, et al (2015) Studies on the role of molybdenum on iodine
880 transport in the RCS in nuclear severe accident conditions. *Annals of Nuclear Energy* 78:117–
881 129. <https://doi.org/10.1016/j.anucene.2014.11.026>
- 882 38. Bahrini C, Grégoire A-C, Obada D, et al (2018) Incoherent broad-band cavity enhanced
883 absorption spectroscopy for sensitive and rapid molecular iodine detection in the presence of
884 aerosols and water vapour. *Optics & Laser Technology* 108:466–479.
885 <https://doi.org/10.1016/j.optlastec.2018.06.050>
- 886 39. vasp.5.4.1

- 887 40. Hafner J (2008) *Ab-initio* simulations of materials using VASP: Density-functional theory and
888 beyond. *Journal of Computational Chemistry* 29:2044–2078. <https://doi.org/10.1002/jcc.21057>
- 889 41. Kresse G, Furthmüller J (1996) Efficiency of ab-initio total energy calculations for metals and
890 semiconductors using a plane-wave basis set. *Computational Materials Science* 6:15–50.
891 [https://doi.org/10.1016/0927-0256\(96\)00008-0](https://doi.org/10.1016/0927-0256(96)00008-0)
- 892 42. Kresse G, Joubert D (1999) From ultrasoft pseudopotentials to the projector augmented-wave
893 method. *Physical Review B* 59:1758–1775. <https://doi.org/10.1103/PhysRevB.59.1758>
- 894 43. Perdew JP, Burke K, Ernzerhof M (1996) Generalized Gradient Approximation Made Simple.
895 *Physical Review Letters* 77:3865–3868. <https://doi.org/10.1103/PhysRevLett.77.3865>
- 896 44. Methfessel M, Paxton AT (1989) High-precision sampling for Brillouin-zone integration in
897 metals. *Physical Review B* 40:3616–3621. <https://doi.org/10.1103/PhysRevB.40.3616>
- 898 45. Monkhorst HJ, Pack JD (1976) Special points for Brillouin-zone integrations. *Physical Review B*
899 13:5188–5192. <https://doi.org/10.1103/PhysRevB.13.5188>
- 900 46. Tkatchenko A, Scheffler M (2009) Accurate Molecular Van Der Waals Interactions from Ground-
901 State Electron Density and Free-Atom Reference Data. *Physical Review Letters* 102:.
902 <https://doi.org/10.1103/PhysRevLett.102.073005>
- 903 47. Riggs CA, Tompson RV, Ghosh TK, et al (2007) Water Adsorption Isotherms for Charged and
904 Uncharged Cesium Iodide Aerosol Particles. *Nuclear Technology* 157:74–86.
905 <https://doi.org/10.13182/NT07-A3803>
- 906 48. Souvi SMO, Badawi M, Virot F, et al (2017) Influence of water, dihydrogen and dioxygen on the
907 stability of the Cr₂O₃ surface: A first-principles investigation. *Surface Science* 666:44–52.
908 <https://doi.org/10.1016/j.susc.2017.08.005>
- 909 49. Sasaki K, Tanigaki T, Tomohiro Oshima, et al (2013) Microstructure Analysis for Chemical
910 Interaction between Cesium and SUS316 Steel in Fast Breeder Reactor Application. *Journal of*
911 *Energy and Power Engineering* 7:716–725. <https://doi.org/10.17265/1934-8975/2013.04.014>
- 912 50. Satpathy S (1986) Electron energy bands and cohesive properties of CsCl, CsBr, and CsI. *Physical*
913 *Review B* 33:8706–8715. <https://doi.org/10.1103/PhysRevB.33.8706>
- 914 51. Sakamoto Y, Yabushita A, Kawasaki M, Enami S (2009) Direct Emission of I₂ Molecule and IO
915 Radical from the Heterogeneous Reactions of Gaseous Ozone with Aqueous Potassium Iodide
916 Solution. *J Phys Chem A* 113:7707–7713. <https://doi.org/10.1021/jp903486u>
- 917 52. Fortin C, Fèvre-Nollet V, Cousin F, et al (2019) Box modelling of gas-phase atmospheric iodine
918 chemical reactivity in case of a nuclear accident. *Atmospheric Environment* 214:116838.
919 <https://doi.org/10.1016/j.atmosenv.2019.116838>

920